Preprints.org

Article

Not peer-reviewed version

The influence of Fe content on the oxidation evolution on Alloy X-750 in simulated BWR environment

Silvia Tuzi , Krystyna Stiller , Mattias Thuvander *

Posted Date: 28 September 2023

doi: 10.20944/preprints202309.1959.v1

Keywords: oxidation; boiling water reactor; spacer; autoclave corrosion testing; nickel base alloys

Preprints.org is a free multidiscipline platform providing preprint service that is dedicated to making early versions of research outputs permanently available and citable. Preprints posted at Preprints.org appear in Web of Science, Crossref, Google Scholar, Scilit, Europe PMC.

Copyright: This is an open access article distributed under the Creative Commons Attribution License which permits unrestricted use, distribution, and reproduction in any medium, provided the original work is properly cited.

Preprints (www.preprints.org) | NOT PEER-REVIEWED | Posted: 28 September 2023 doi:10.20944/preprints202309.1959.v1

Disclaimer/Publisher's Note: The statements, opinions, and data contained in all publications are solely those of the individual author(s) and contributor(s) and not of MDPI and/or the editor(s). MDPI and/or the editor(s) disclaim responsibility for any injury to people or property resulting from any ideas, methods, instructions, or products referred to in the content.

Article

The Influence of Fe Content on the Oxidation Evolution on Alloy X-750 in Simulated BWR Environment

Silvia Tuzi, Krystyna Stiller and Mattias Thuvander *

Department of Physics, Chalmers University of Technology, 412 96 Gothenburg, Sweden
* Correspondence: mattias.thuvander@chalmers.se

Abstract: This paper presents an investigation of the oxidation of Alloy X-750 containing 5% Fe in a simulated boiling water reactor (BWR) environment. To mimic the conditions in which the bare metal is exposed to the reactor water the samples were not pre-oxidized. The specimens were exposed for durations ranging from 2 to 840 hours, and the development of the oxide microstructure was mainly studied using electron microscopy. The results showed that the oxide scale consisted of blocky crystals of trevorite on top of a porous inner layer rich in Ni and Cr. After the longest exposure time, the trevorite crystals completely covered the specimen surface. The study further revealed that the speed at which the oxide grew and the metal dissolved both decreased with time. Additionally, the metal thinning process was found to be sub-parabolic. Given the significant variation in iron content in the X-750 specification, the influence of this element on the material's corrosion performance in BWR was examined by comparing the results from this investigation with those from previous work on material containing 8 wt% Fe. The study demonstrated that the oxide growth, metal dissolution and metal thinning were slower in the material with higher Fe content, indicating the importance of this element in limiting the degradation of Alloy X-750 in BWR environments.

Keywords: oxidation; boiling water reactor; spacer; autoclave corrosion testing

1. Introduction

Alloy X-750 is a precipitation hardened Ni-Cr-Fe superalloy with an iron content specified to lie within the range of 5-9 wt%. It is known for its very good corrosion resistance and high strength at high temperatures, making it an ideal choice for use in nuclear power plants. Thus, for more than three decades, it has been used for various applications, including springs, bolts, welds, and spacer grids used to hold the fuel material. However, the harsh boiling water reactor (BWR) environment characterized by high-temperature water, radiolysis products, and corrosive electropotential, exposes Alloy X-750 to uniform corrosion and mass loss. Corrosion resistance is one of the primary properties required to be screened for reactor materials. However, tests of X-750 in water or steam simulating reactor conditions are scant and most of these investigations are directed towards material degradation through stress corrosion cracking [1-6] while there are only few reports focusing on its uniform corrosion [7-9].

To mitigate corrosion, the X-750 alloy typically undergoes pre-treatment, consisting of a heat treatment at 700 °C for 20 hours. This pre-treatment results, besides the development of strengthening γ'-Ni_3(Ti,Al) precipitates, in formation of a thin layer of protective oxide scale. Analysis of this oxide reveals that it comprises a $NiFe_2O_4$ spinel layer growing on top of a Cr_2O_3 layer [7]. However, it is still possible that this protective oxide layer is consumed or damaged during operation in the reactor core and a bare metal would be exposed. It is thus essential to understand also the corrosion behavior of the alloy in non-pre-oxidized condition.

Previous investigations of non-pre-oxidized alloy X-750 exposed to a simulated BWR environment showed that the oxide scale consists of more than one layer. Chen et al. [8] demonstrated that the scale formed on the alloy with 7.5 wt% Fe exposed to a simulated BWR environment for 840 h consisted of trevorite crystals formed on top of a duplex inner oxide of $NiCrO_3$ and NiO. Our

© 2023 by the author(s). Distributed under a Creative Commons CC BY license.

Preprints (www.preprints.org) | NOT PEER-REVIEWED | Posted: 28 September 2023 doi:10.20944/preprints202309.1959.v1

previous work on the evolution of the oxide scale on non-pre-oxidized alloy X-750 with 8 wt% Fe (8Fe) exposed to simulated BWR conditions for periods ranging from 2 to 840 h reveals that the oxide scale starts as a bi-layered structure of blocky $NiFe_2O_4$ crystals on a Ni- and Cr-rich layer. With longer exposure times, it develops into a penta-layered configuration ($NiFe_2O_4$, Ti-rich mixed spinel, NiO, Cr-enriched oxidized metal, and oxidized metal). Moreover, porosity was observed within the scale after short exposures, but eventually, the voids were filled with longer exposures [9].

It is known that the iron content in Ni-Cr-Fe alloys alters the material corrosion performance in pressurized water reactor (PWR) water environment [10]. Thus, given the quite wide range of iron content in the specification of X-750, it is important to scrutinize the influence of this element on the oxidation performance of the alloy in simulated BWR environment. Here we are presenting the results of an investigation in which we studied non-pre-oxidized alloy X-750 with a lower iron content, 5 wt% Fe (5Fe), primarily using electron microscopy. Our approach was similar to that used in reference [9]. A comparison between the 5Fe and 8Fe materials is made, and a corrosion course of events is suggested.

2. Materials and Methods

Specimens of Alloy X-750 were taken from strip manufacturing and their chemical composition is shown in Table 1. Sample coupons of size 20x20x0.3 mm^3 were cut from the strip and then placed in a titanium-plated autoclave for exposure to high-temperature water. The autoclave setup was identical to that used in our previous work [9]. To replicate the conditions in a BWR, the temperature was set to 286 °C under a pressure of 80 bar. To simulate water radiolysis, a continuous addition of 500 ppb of H_2O_2 was made to the loop, and a water jet was set to impinge the specimens at 10 m/s. Four different exposure times were chosen: 2, 24, 168 and 840 h. These specimens are henceforth referred to as 5Fe-2h, 5Fe-24h, 5Fe-168h and 5Fe- 840h, respectively.

Prior to and following each exposure, an analytical balance with 0.1 mg precision was used to weight the specimens.

The specimen surface was analysed with X-ray diffraction (XRD) measurements at ambient temperature using a Siemens D5000 diffractometer in a grazing incidence set-up (7.5° theta) in detector scan mode with a Göbel mirror and an energy dispersive detector. XRD analysis was performed over the 2θ range of 15 – 80°, with a step size of 0.009° and 2 s collection time per step using Cu-Kα (wavelength = 1.54 Å) radiation. After background subtraction and a Fourier smoothing, phases were identified using the DIFFRACplusEVA evaluation software package with SEARCH, using ICDD database 2014 for phase identification. Moreover, high resolution XRD measurements were also carried out in a Bruker AXS D8 ADVANCE VARIO powder diffractometer using monochromatic Cu-Kα1 (1.54 Å) to check the possible presence of any other phases.

Top view images of the specimens were taken with a scanning electron microscope Leo Ultra 55 FEG-SEM. A focused ion beam (FIB) combined with an SEM of type FEI Versa 3D FIB/SEM was utilized to create cross-sections and lift-out lamellas and to obtain the 3D structure of oxide in a slice-and-view experiment. An FEI Titan 80-300 TEM/STEM (EDX system by Oxford Instruments) was employed to produce high resolution images using high-angle annular dark field scanning transmission electron microscopy (HAADF-STEM). Energy dispersive x-ray (EDX) technique was used to obtain elemental maps.

Table 1. Chemical composition of Alloy X-750 with two different Fe contents, the composition is given in both at.% and wt%.

Material	C	Si	Mn	Cr	Ni	Nb+Ta	Ti	Al	Fe
Fe5 (wt%)	0.02	0.34	0.54	15.6	73.9	0.8	2.5	0.9	5.4
Fe8 (wt%)	0.02	0.35	0.57	16.0	70.8	0.8	2.4	0.6	8.3
Fe5 (at.%)	0.10	0.69	0.56	17.0	71.2	0.34	2.9	1.9	5.3
Fe8 (at.%)	0.10	0.71	0.59	17.6	68.5	0.34	2.8	1.3	8.2

Preprints (www.preprints.org) | NOT PEER-REVIEWED | Posted: 28 September 2023 doi:10.20944/preprints202309.1959.v1

3. Results

The mass changes of the 5Fe samples are presented in Figure 1 together with the 8Fe samples [9]. For all the exposure times, the mass change is negative, meaning that material is lost into the water. In Figure 2, the results from XRD analyses (using grazing incident measurements) of the specimens exposed for 2, 24 and 168 h are depicted with characteristic peaks for $NiFe_2O_4$ spinels (trevorite) evident only after the 168 h exposure. The same phases were identified by powder diffractometry.

Top view SEM images acquired with secondary electrons are presented in Figure 3. The 5Fe-2h sample is covered with nano-sized particles (5-40 nm) with a coverage of about 3%, while on 5Fe-24h oxide particles cover about 20% of the surface area. The crystal size varies, with sizes reaching up to 500 nm. On 5Fe-168h, two types of crystals are discernible, with large crystals (0.5-1.5 μm) present on top of smaller ones. The coverage of the larger crystals is evaluated to be about 50%. Based on XRD analysis, it is assumed that the crystals are trevorite. The oxide layer beneath the spinels consists of crystals of different shapes; needle- and plate-like. Sample 5Fe-840h shows crystals fully covering the surface, and the crystal size reaches up to 2 μm.

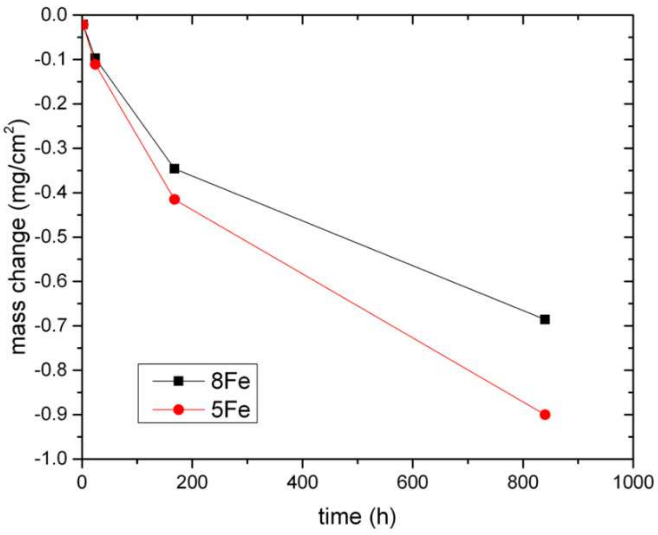

Figure 1. Mass change as function of exposure time.

Preprints (www.preprints.org) | NOT PEER-REVIEWED | Posted: 28 September 2023 doi:10.20944/preprints202309.1959.v1

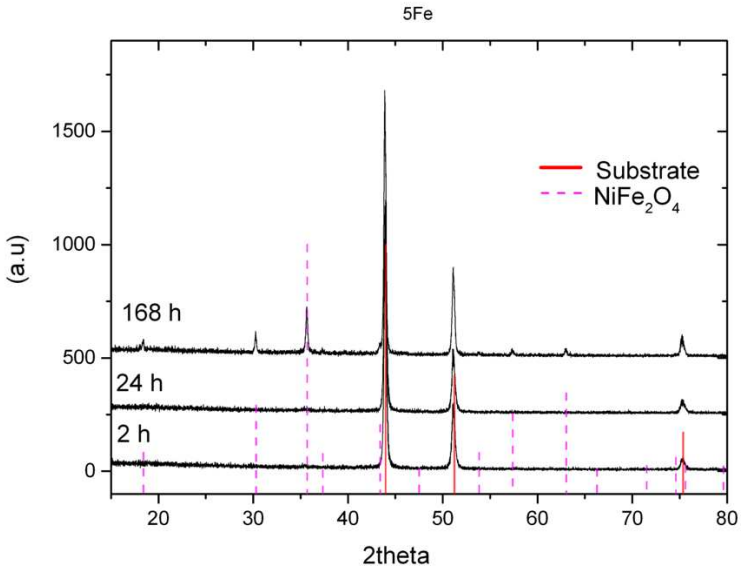

Figure 2. XRD analysis of the specimens exposed to simulated boiling water reactor environment. The only detectable phase, apart from the substrate, is trevorite $NiFe_2O_4$.

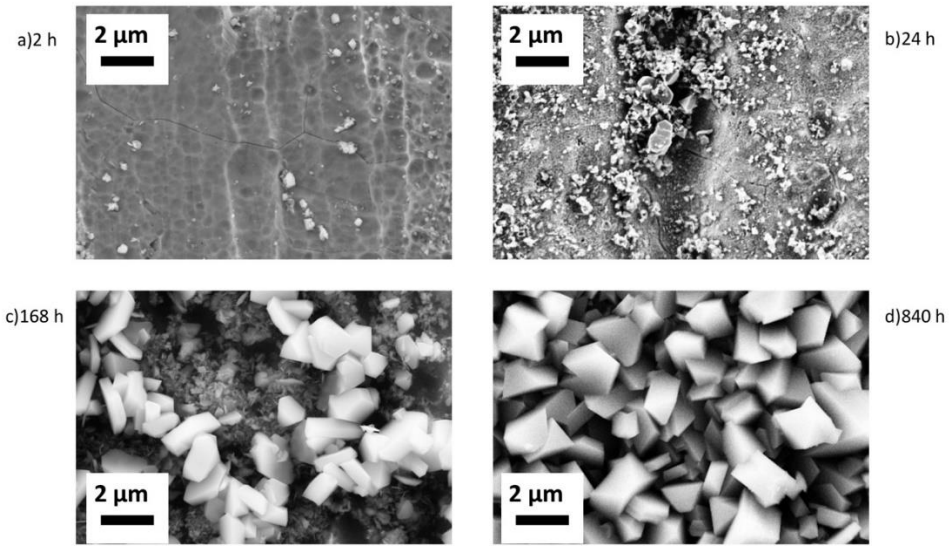

Figure 3. SEM top view images of specimens exposed to simulated boiling water reactor environment: (**a**) 5Fe-2h; (**b**)5Fe- 24h; (**c**) 5Fe-168h; (**d**) 5Fe-840h. The evolution of the oxide from nano-sized particles covering only 3% of the surface to full coverage of the surface after 840 h with crystals of 1-2 µm is visible.

From the FIB cross sections displayed in Figure 4, it is observed that on 5Fe-168h, the oxide-metal interface is porous, resulting in the oxide being attached to the surface only in a small fraction of the area. This made the preparation of FIB lift-out cross sections for TEM very laborious. The oxide is 1.7 ± 0.2 µm thick, and from the cross section in Figure 4a, three layers can be distinguished; an outer layer made of trevorite, a middle layer made of plate-like oxide, and a continuous inner layer.

After 840 h, Figure 4b, the oxide is less porous and noticeably thicker, 2.7 ± 0.2 µm. The scale appears to consist of three layers from this image: a thick and continuous trevorite layer, a middle layer consisting of smaller grains and an inner layer of fine-grained oxide.

Preprints (www.preprints.org) | NOT PEER-REVIEWED | Posted: 28 September 2023 doi:10.20944/preprints202309.1959.v1

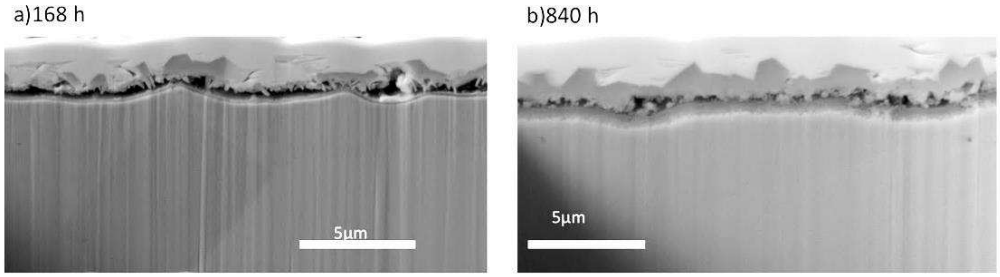

Figure 4. FIB cross section of specimens exposed in simulated boiling water reactor environment (**a**) 5Fe-168h; (**b**) 5Fe-840h.

To gain a better understanding, HAADF-STEM images were acquired, and the cross sections of the different specimens are presented in Figure 5. The specimen 5Fe-2h has a few nanoparticles imbedded in the Pt layer (deposited as protection with FIB), while the trevorite is clearly present on the specimen 5Fe-24h. Figure 5c shows the porous nature of the oxide on 5Fe-168h. Spinel crystals and needle-like crystals covering a fine-grained oxide layer approximately 200 nm thick can be distinguished. Investigation of 5Fe-840 h shows, as expected from the FIB cross section, that below the large spinel crystals, a layer of smaller crystals is present. Pores are still present, and an inner fine-grained oxide layer of approximately 500 nm (i.e., thicker than for the specimen 5Fe-168h) is visible.

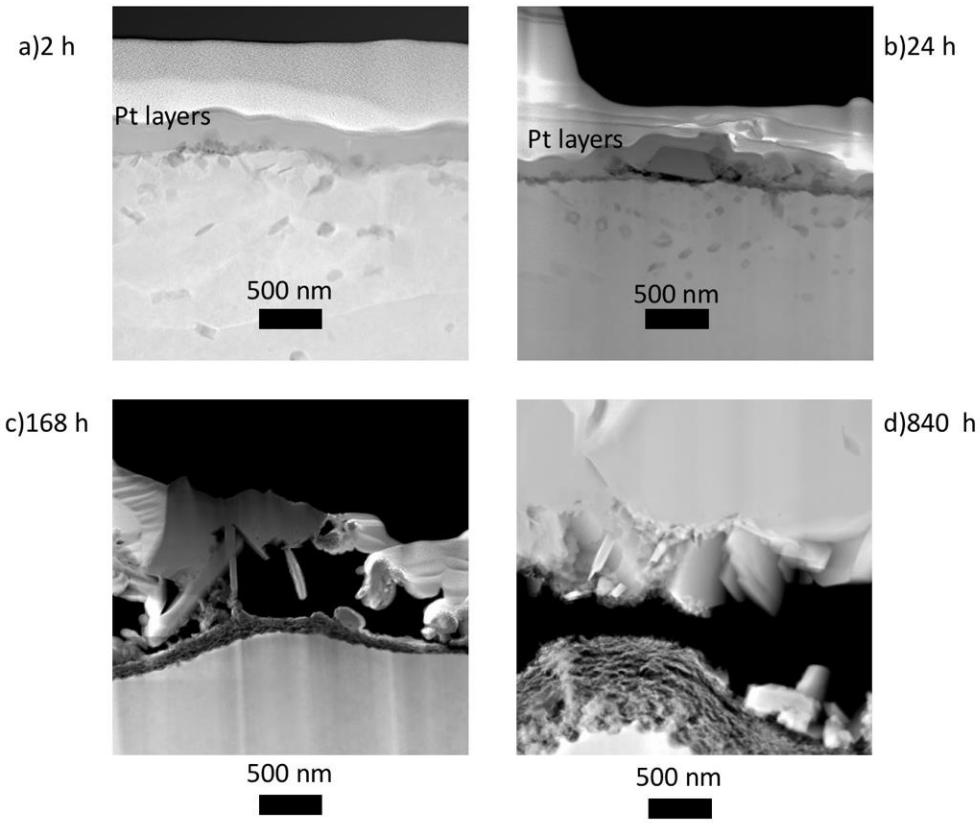

Figure 5. HAADF-STEM images of specimens exposed in simulated boiling water reactor environment: (**a**) 5Fe-2h; (**b**)5Fe-24h; (**c**) 5Fe-168h; (**d**) 5Fe- 840h.

To obtain chemical information from the oxide scale for the different exposure times, STEM-EDX maps were acquired. Figure 6 shows EDX maps of 5Fe-24h. After this exposure, the $NiFe_2O_4$ crystals are not stoichiometric since the ratio between Ni and Fe is close to 1. Beneath the spinel crystals, a thin oxide layer rich in Cr and Ni can be observed. After 168 h, the oxide scale consists of

Preprints (www.preprints.org) | NOT PEER-REVIEWED | Posted: 28 September 2023 doi:10.20944/preprints202309.1959.v1

three layers, as shown in Figure 7. According to the EDX maps, there are plate-like crystals rich in Ni, Fe and Ti between the spinel layer and the fine-grained oxide. When the specimen has been exposed for 840 h, the EDX maps in Figure 8 reveal a three-layer structure, trevorite in the upper part, NiO in the middle part and a fine-grained Ni- and Cr-rich oxide inner layer. The NiO inner layer is very porous, however, it is more adherent to the surface than in 5Fe-168h.

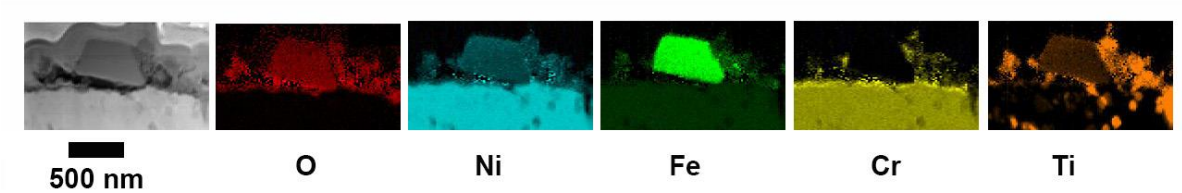

Figure 6. HAADF-STEM EDX map of 5Fe-24h.

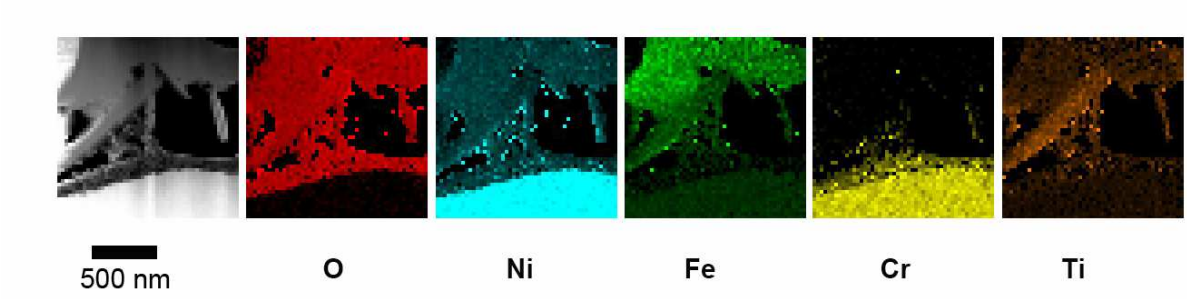

Figure 7. HAADF-STEM EDX map of 5Fe-168h.

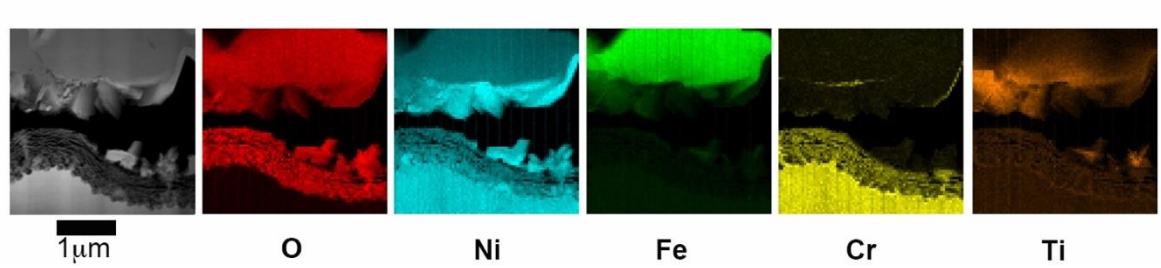

Figure 8. HAADF-STEM EDX map of 5Fe-840h.

To examine the 3D structure of the voids, present in the oxide scale, a slice-and-view experiment was conducted on the specimen 5Fe-840h. The aim was to determine whether the thick layer of trevorite is protective or if it contains void channels that allow water to easily access the metal. Figure 9 shows a sequence of cross-sections of the examined volume. Void channels are visible in the trevorite layer, indicating that water can penetrate through to the metal. However, some areas of the trevorite layer have limited porosity. The middle layer's porosity is very interesting since it has large empty areas attached to the surface only with very small crystals. In other areas, that are more adherent to the specimen, many small pores are observed. These findings agree with the results of the TEM investigation and demonstrate the local porosity of the oxide scale.

Preprints (www.preprints.org) | NOT PEER-REVIEWED | Posted: 28 September 2023 doi:10.20944/preprints202309.1959.v1

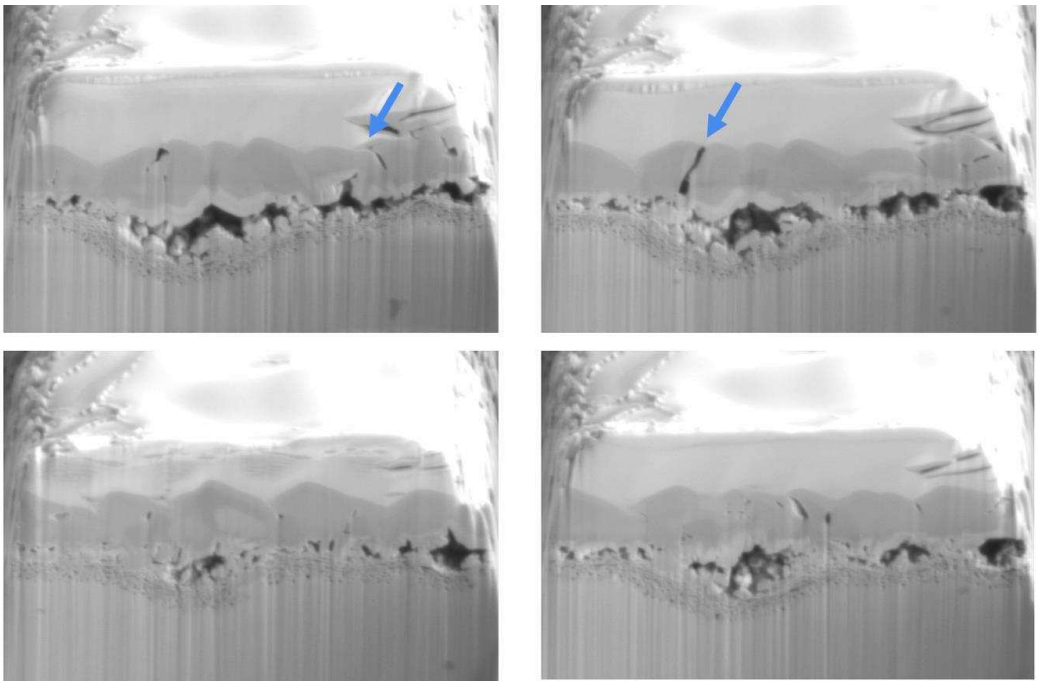

Figure 9. SE Images of 5Fe exposed for 840 h. The images are part of a slice and view video, where the 3D structure of the oxide scale is shown. Arrows point out channels for water.

4. Discussion

The purpose of this paper is to compare X-750 specimens containing 5 wt% Fe with specimens containing 8 wt% Fe from our previous work [9] when exposed in a simulated BWR environment.

The observed oxide evolution is similar to that observed in our previous work on 8Fe [9]. The structure of the oxide scale is also comparable to that found in a study made on X-750 with 7.5 wt% Fe [8], where the oxide was relatively thick, with an outer layer of trevorite crystals of 7 μm and a duplex inner oxide of 0.8 μm of $NiCrO_3$ and NiO [8]. However, the different flow velocity (18 m/s) used in that investigation makes it quite challenging to correlate the results with our finding.

The mass change results in Figure 1 indicate that the two materials have comparable mass losses for short exposure times (2 and 24 h), but begin to deviate after 168 h. After 840 h, the material containing 5Fe has lost about 32% more mass. The mass loss suggests a degradation process involving the dissolution of metal ions with a concomitant oxide formation. An estimation of the dissolved metal thickness lost into the water was made based on the model presented previously [9], which assumes that the mass after exposure equals the sum of the remaining metal mass and the oxide mass. Thus:

$$\Delta m = m(0) - m(t) = m(0) - m(t)_{\text{metal}} - m(t)_{\text{oxide}}. \quad (1)$$

The $m(0)$is the mass measured before the exposure, $m(t)$ is the mass measured after the exposure, the $m(t)_{\text{metal}}$ is the mass of the metal left after exposure, $m(t)_{\text{oxide}}$ is the mass of the total oxide scale gained at time t. The oxide mass is given by $m(t)_{\text{oxide}} = x_{\text{oxide}} A\rho_{\text{oxide}}$, where ρ_{oxide} is the density of the oxide, x_{oxide} is the oxide thickness, and A is the surface area of the test coupon. For the sake of simplicity, we have assumed that the oxide was composed of two layers for each exposure time: the outermost layer made of $NiFe_2O_4$ (with density of 5.3 g/cm³) [11] and the innermost layer made of NiO (with density 6.67 g/cm³) [12]. To calculate the thickness of the dissolved metal, h, after a given exposure time t, we use the following equation:

$$h = \frac{1}{A\rho X750}\left(\Delta m + 0.27 x_{NiFe_2O_4} A\rho_{NiFe_2O_4} + 0.21 x_{NiO} A\rho_{NiO}\right). \quad (2)$$

In the formula, the density of the alloy is ρ_{X750} = 8.2 g/cm³ and x is the measured average thickness from TEM image analysis. The factor 0.27 represents the mass fraction of oxygen if $NiFe_2O_4$ has an ideal composition, and 0.21 is the same factor if NiO has an ideal composition. In Figure 10, the

Preprints (www.preprints.org) | NOT PEER-REVIEWED | Posted: 28 September 2023 doi:10.20944/preprints202309.1959.v1

calculated dissolved thickness of the metal and the measured oxide thickness are presented for the 5Fe material, as function of the exposure time. The specimen exposed for 24 h dissolves about 0.5 µm while an oxide of about 0.8 µm is found on the surface. After 168 h, 1.2 µm has been dissolved into the water and an oxide of 1.7 µm has been built. When 840 h have passed, the metal thickness dissolved into the water reaches almost 2.5 µm and the built-up oxide is 2.7 µm thick. In Figure 11, a comparison between the two materials with respect to the measured oxide thickness is presented, the oxide formed on the 5Fe material is noticeably thicker after 840 h.

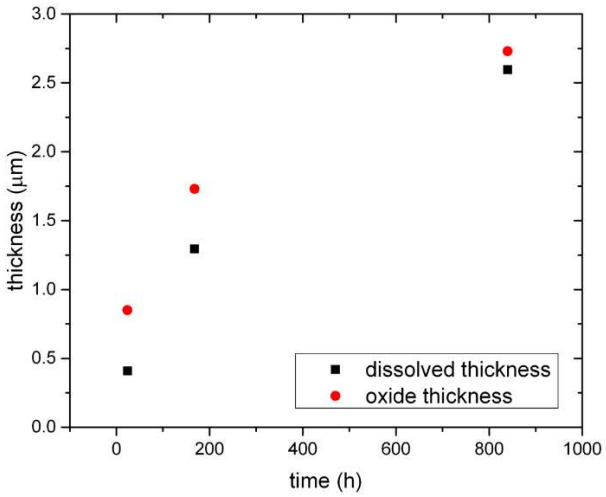

Figure 10. Calculated thickness of the dissolved metal and measured oxide thickness for 5Fe.

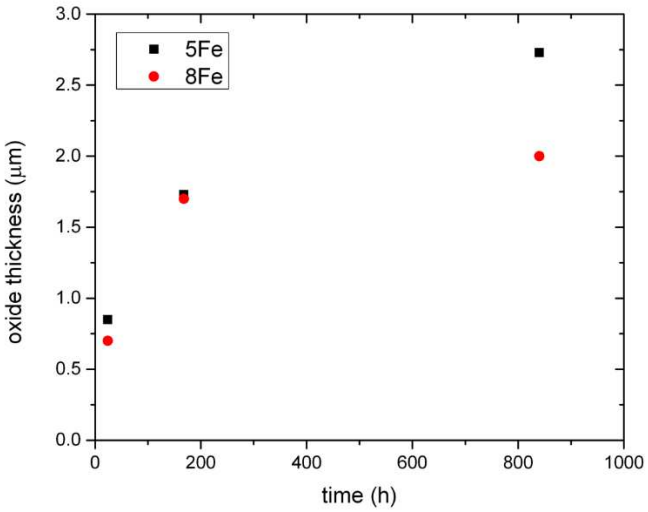

Figure 11. Comparison of the measured oxide thickness for 5Fe and 8Fe as function of exposure time.

When comparing the dissolution rate of the two batches with different Fe content, in Figure 12, it is evident that the 5Fe material loses more metal after 840 h than 8Fe. Calculations of the metal thinning are reported in Figure 13. The metal thinning is calculated as:

$$h' = \frac{1}{A\rho X750}\left(\Delta m + x_{NiFe_2O_4} A\rho_{NiFe_2O_4} + x_{NiO} A\rho_{NiO}\right). \quad (3)$$

Preprints (www.preprints.org) | NOT PEER-REVIEWED | Posted: 28 September 2023 doi:10.20944/preprints202309.1959.v1

This formula differs from equation 1, which is used to calculate the dissolved thickness. Unlike equation 1, this formula considers the total amount of thickness lost into the water without taking into account the oxygen rescaling resulting from the formation of the oxide. For instance, after 840 h, the metal thinning for 5Fe is 3.7 μm, while the corresponding dissolved thickness is 2.5 μm. This means that 1.2 μm of the metal that went into the water has re-precipitated to form the oxide scale.

From curve fitting, Figure 13, we observe that the metal thinning behaviour follows a sub-parabolic trend. The metal thinning for 5Fe and 8Fe, with metal thinning in μm and exposure time t in hours, is given by:

$$h'_{5Fe} = 0.25t^{0.41} \quad (4)$$

$$h'_{8Fe} = 0.28t^{0.37}. \quad (5)$$

The inset in Figure 13 illustrates the derivative of the metal thinning. The metal thinning rate as a function of time tends to decrease with time, indicating that the metal thinning rate will eventually become constant. However, longer exposure times should be performed to verify this hypothesis.

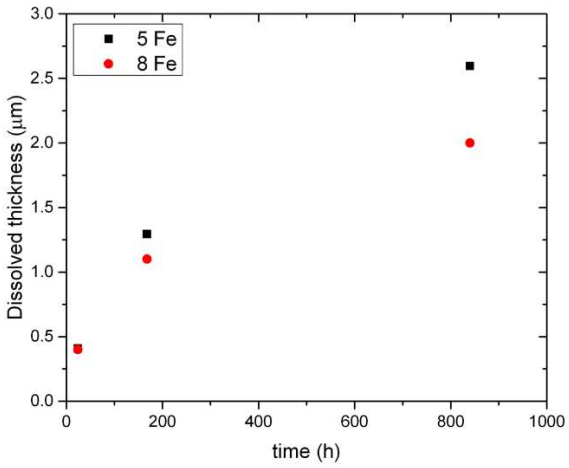

Figure 12. Comparison of calculated thickness of the dissolved metal for 5Fe and 8Fe as function of exposure time.

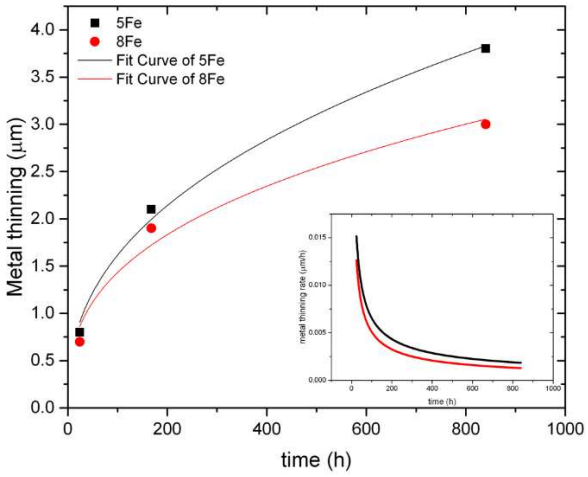

Figure 13. Metal thinning as function of exposure time. In the inset the metal thinning rate is showed. It is suggested that the rate will became constant for longer exposures.

Preprints (www.preprints.org) | NOT PEER-REVIEWED | Posted: 28 September 2023 doi:10.20944/preprints202309.1959.v1

5. Conclusions

In conclusion, this paper presents a study of the influence of Fe on the oxidation behaviour of non-pre-oxidized Alloy X-750. Two batches of Alloy X-750, containing 5 wt% and 8 wt% Fe, were compared. Both materials experienced mass loss during the autoclave exposures carried out for durations ranging from 2 to 840 hours. The oxide growth was similar for both batches, beginning with trevorite nanoparticles after 2 h, and progressing to a more complex oxide, after 840 h, consisting of an outer layer of $NiFe_2O_4$, a middle layer of NiO and a fine-grained inner layer rich in Ni and Cr. The oxide thickness of the two batches was quite similar until 168 h, after which time the oxide growth was faster for the 5Fe batch. Moreover, the oxide found on the 5Fe material was less adherent to the surface and more porous. Calculations revealed that the rate at which the oxide grows and the rate at which the metal dissolves both decrease with time, and that the metal thinning is a sub-parabolic process. The three processes were slower for the material with higher Fe content, 8 wt%, demonstrating the importance of this element in limiting the degradation of Alloy X-750 in BWR environments.

Author Contributions: Conceptualization, K.S. and M.T.; investigation, S.T.; resources, K.S..; writing—original draft preparation, S.T.; writing—review and editing, K.S and M.T.; supervision, M.T.; project administration, M.T.; funding acquisition, K.S. All authors have read and agreed to the published version of the manuscript.

Funding: This research was funded by the Swedish Research Council, grant number 2009-3333, and Westinghouse Electric Sweden AB, Sandvik Materials Technology AB, Vattenfall AB and EPRI.

Data Availability Statement: Not applicable.

Acknowledgments: Westinghouse Electric Sweden is acknowledged for providing the material for this study. The experimental work presented in this paper was performed at Chalmers Materials Analysis Laboratory (CMAL).

Conflicts of Interest: The authors declare no conflict of interest. The funders had no role in the design of the study; in the collection, analyses, or interpretation of data; in the writing of the manuscript; or in the decision to publish the results.

References

1. Jensen, A.; Efsing, P.; Sandberg, J. Influence of heat treatment, aging, and neutron irradiation on the fracture toughness and crack growth rate in BWR environments of alloy X-750. In Proceedings of the 12th International Conference on Environmental Degradation of Materials in Nuclear Power Systems – Water Reactors, Salt Lake City, US, 14-18 August 2005.
2. James, L.A. Effect of fast neutron irradiation on fatigue crack growth behaviour of three nickel-base alloys. *Nucl. Tech.* **1981**, *53*, 64-68.
3. Fisher, K.; Teysseyre, S.; Marquis, E.A. Multi Scale Characterization of Stress Corrosion Cracking of Alloy X750. *MRS Online Proceedings Library* **2013**, *1519*, 1002.
4. Grove, C.A.; Petzold, L.D. Mechanisms of Stress-corrosion cracking of alloy X-750 in high-purity water. J. *Mater. Energy Syst.* **1985**, *7*, 147-162.
5. Andresen, P.L.; Flores-Preciado, J.; Morra, M.M.; Carter, R. Microstructure and SCC of Alloy X-750. In Proceedings of the 15th International Conference on Environmental Degradation of Materials in Nuclear Power Systems – Water Reactors, Colorado Springs, US, 7-11 August 2011.
6. Gibbs, J.P.; Ballinger, R.G.; Jackson, J.H.; Isheim, D.; Hänninen, H. Stress Corrosion Cracking and Crack Tip Characterization of Alloy X-750 in Boiling Water Reactor Environments. In Proceedings of the 15th International Conference on Environmental Degradation of Materials in Nuclear Power Systems – Water Reactors, Colorado Springs, US, 7-11 August 2011.
7. Tuzi, S.; Lai, H.; Göransson, K.; Thuvander, M.; Stiller, K. Corrosion of preoxidized nickel alloy X-750 in simulated BWR environment. *J. Nucl. Mater.* **2017**, *486*, 350-360.
8. Chen, J.; Lindberg, F.; Belova, L.; Forssgren, B.; Gott, K.; Lejon, J.; Jasiulevicius, A. High Resolution Electron Microscopy Study on Oxide FilmsFormed on Nickel-Base Alloys X-750, 182 and 82 in Simulated High Flow Velocity BWR Water. In Proceedings of the 15th International Conference on Environmental Degradation of Materials in Nuclear Power Systems – Water Reactors, Colorado Springs, US, 7-11 August 2011.

Preprints (www.preprints.org) | NOT PEER-REVIEWED | Posted: 28 September 2023 doi:10.20944/preprints202309.1959.v1

9. Tuzi, S.; Göransson, K.; Rahman, S.M.H.; Eriksson, S.G.; Liu, F.; Thuvander, M.; Stiller, K. Oxide evolution on Alloy X-750 in simulated BWR environment. *J. Nucl. Mater.* **2016**, *482*, 19-27.
10. Ru, X.; Ma, J.; Lu, Z.; Chen, J.; Han, G.; Hu, J.Z.P; Liang, X.; Tang, W. Effects of iron content in NieCreFe alloys on the oxide films formed in an oxygenated simulated PWR water environment. *J. Nucl. Mater.* **2018**, *509*, 29-42.
11. Deer, W.A.; Howie, R.A.; Zussman, J.; Bowles, J.F.W.; Vaughan, D.J., *Rock-Forming Minerals: Non-Silicates: Oxides, Hydroxides and Sulphides*, 2nd ed.; Geological Society of London: London, UK, 2011.
12. Weast, R,C., *CRC Handbook of Chemistry and Physics*,55th ed.; CRC Press: Boca Raton, US, 1974.

Disclaimer/Publisher's Note: The statements, opinions and data contained in all publications are solely those of the individual author(s) and contributor(s) and not of MDPI and/or the editor(s). MDPI and/or the editor(s) disclaim responsibility for any injury to people or property resulting from any ideas, methods, instructions or products referred to in the content.